A C-13 and H-1 NMR spectroscopic investigation of the structure of the iminium ion with a dipolar form in metal complexes of 2-N-substituted N-confused porphyrins

ARTICLE *in* DALTON TRANSACTIONS · SEPTEMBER 2012

Impact Factor: 4.2 · DOI: 10.1039/c2dt31426f · Source: PubMed

5 AUTHORS, INCLUDING:

Jyh-Horung Chen
National Chung Hsing University
86 PUBLICATIONS **650** CITATIONS

SEE PROFILE

Dalton Transactions

Cite this: *Dalton Trans.*, 2012, **41**, 13454

www.rsc.org/dalton

PAPER

A ^{13}C and ^{1}H NMR spectroscopic investigation of the structure of the iminium ion with a dipolar form in metal complexes of 2-N-substituted N-confused porphyrins†

Wen-Pin Chang,[a] Wen-Chain Lin,[a] Jyh-Horung Chen,*[a] Shin-Shin Wang[b] and Jo-Yu Tung[c]

Received 2nd July 2012, Accepted 5th September 2012
DOI: 10.1039/c2dt31426f

The crystal structures of chloro(2-aza-2-ethoxycarbonylmethyl-5,10,15,20-tetraphenyl-21-carbaporphyrinato-*N*,*N*′*N*″) zinc(II) [Zn(2-$NCH_2COOC_2H_5$NCTPP)Cl; **4**], (2-aza-2-ethoxycarbonylmethyl-5,10,15,20-tetraphenyl-21-carbaporphyrinato-*N*,*N*′*N*″) palladium(II) [Pd(2-$NCH_2COOC_2H_5$NCTPP); **5**], bromo(2-aza-2-ethoxycarbonylmethyl-5,10,15,20-tetraphenyl-21-carbaporphyrinato-*N*,*N*′*N*″) manganese(III) [Mn(2-$NCH_2COOC_2H_5$NCTPP)Br; **6**], [2-aza-(3′-phenoxypropyl)-5,10,15,20-tetraphenyl-21-carbaporphyrinato-*N*,*N*′*N*′] nickel(II) [Ni(2-$NCH_2CH_2CH_2OC_6H_5$NCTPP); **7**] and chloro(2-aza-2-methoxycarbonylmethyl-5,10,15,20-tetraphenyl-21-carbaporphyrinato-*N*,*N*′*N*″) zinc(II) [Zn(2-NCH_2COOCH_3NCTPP)Cl; **8**] have been established. The *g* value of 9.54, which was measured from the parallel polarization of the X-band EPR spectra in $CHCl_3$ at 4 K, is consistent with the high spin mononuclear manganese(III) centre ($S = 2$) in **6**. The magnitude of the axial (*D*) zero-field splitting (ZFS) for the mononuclear Mn(III) centre in **6** was determined approximately to be 1.63 cm^{-1} by paramagnetic susceptibility measurements. The NMR spectroscopic investigation of the iminium ion with a dipolar canonical contribution to the metal complexes **5–7**, Pd(2-$NCH_2C_6H_5$NCTPP) (**10**) and Ni(2-$NCH_2C_6H_5$NCTPP) (**11**) in $CDCl_3$ is reported. A resonance between the dipolar canonical form **II** and covalent canonical form **I** exists for complexes **5–7**, **10** and **11** in $CDCl_3$. To develop the correlations between $\delta^{13}C$ [C(3)], $\delta^{1}H$ [H(3)] and the canonical form **II** in **5–7**, **10** and **11**, this work thoroughly examines the ^{13}C and ^{1}H NMR of N^+=CH(Ar) fragment on seven metal complexes of 2-N substituted N-confused porphyrin. According to these results, the ^{13}C [C(3)] and ^{1}H [H(3)] chemical shifts of the N^+=CH(Ar) fragment at 20 °C in $CDCl_3$ are separately located at 152.6 ± 0.5 and 8.30 ± 0.15 ppm respectively for the iminium ion. This exists as a dipolar canonical form **II** for complexes **5–7**, **10** and **11**, and the N–CH(Ar) group appears at 121.1 ± 0.1 ppm and 6.35 ± 0.01 ppm, which is in a covalent canonical form **I** contribution to complexes **4** and **8**. X-Ray diffraction data indicate that N(2)–C(3) = 1.315 ± 0.011 Å for the dipolar contribution of **5–7**, **10–13**, while N(2)–C(3) = 1.331 ± 0.008 Å for the covalent contribution of **4** and **8**.

Introduction

An N-confused porphyrin NCP is a porphyrin isomer with an inverted pyrrole ring. There are three main reaction sites in the confused pyrrole ring, *i.e.*, 2-N, 21-C and 3-C (Scheme 1).[1]

Substitution of the position 3-C is catalyzed by acids.[1,2] At the external nitrogen of NCP (2-N), an electrophilic reaction can take place resulting in the formation of alkylation products. Ziegler and co-workers reported the synthesis of the 2-aza-2-ethoxycarbonylmethyl-5,10,15,20-tetraphenyl-21-carbaporphyrin 2-NCH_2COOEtNCTPPH (**1**).[3] When the ethoxycarbonylmethyl group of **1** is modified to a bulky 3′-phenoxypropyl group, the free base 2-aza-(3′-phenoxypropyl)-5,10,15,20-tetraphenyl N-confused porphyrin, 2-$NCH_2CH_2CH_2OC_6H_5$NCTPPH (**2**), is derived.[4] In this study, we focus on the alkyl group of 2-NCH_2COOEtNCTPPH (**1**) and 2-$NCH_2CH_2CH_2OC_6H_5$-NCTPPH (**2**).[4] Unlike the NH tautomerism that exists in

[a]*Department of Chemistry, National Chung Hsing University, Taichung 40227, Taiwan. E-mail: JyhHChen@dragon.nchu.edu.tw; Fax: +886 422862547; Tel: +886 422840412x612*
[b]*Material Chemical Laboratories ITRI, Hsin-Chu 300, Taiwan. E-mail: ShinShinWang@ITRI.org.tw; Tel: +886 35732550*
[c]*Department of Occupational Safety and Health, Chung Hwai University of Medical Technology, Taiwan. E-mail: joyuting@mail.hwai.edu.tw; Fax: +886 62894028; Tel: +886 62674567x815*

†Electronic supplementary information (ESI) available: Fig. S1 showing the atom number scheme for **2**, **7**. Fig. S2 (or Fig. S3) showing the atom numbering scheme for **4**, **8** (or **5**, **6**), respectively. Fig. S4 (or Fig. S5) showing the ^{1}H NMR spectra for **8** (or **7**) in $CDCl_3$ at 20 °C. Fig. S6 showing the UV/visible spectrum for **7** in CH_2Cl_2 at 20 °C. Fig. S7 (or Fig. S8) showing the UV/visible spectra for **4**, **8** (or **5**, **6**), respectively, in CH_2Cl_2 at 20 °C. CCDC 889011–889015. For ESI and crystallographic data in CIF or other electronic format see DOI: 10.1039/c2dt31426f

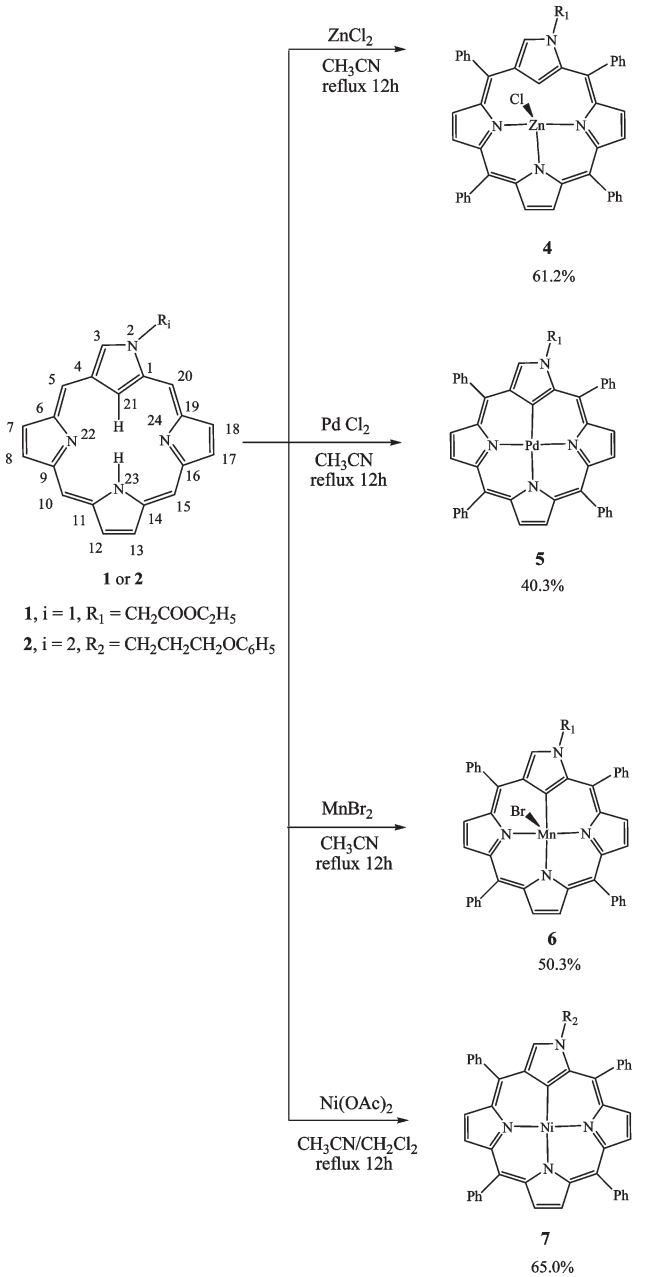

Scheme 1 Synthesis of **4**, **5**, **6** and **7**.‡

NCTPPH$_2$, the free base **1** (or **2**) has only one stable form. The N-confused porphyrin **1** (or **2**) can provide N_3 or N_3C coordinated sites. Hitherto, free base **1** has been shown to coordinate with metals in the core thereby forming a metal complex possessing a carbon–metal bond for Co(II) (I = 7/2) in Co(2-NCH$_2$COOEtNCTPP)py (**3**) [or Co(NCTPP-AcOEt)py, Co(NCTPP-CH$_2$COOEt)py].[3] In order to investigate the range of metal ions that can be inserted into **1**, we have extended our studies on the insertion of zinc, palladium and manganese into **1**.

‡The numbering scheme on the far left of Scheme 1 is used for the nomenclature of the compounds and this numbering scheme is consistent with the report in the literature. Moreover, the NMR data assignment uses the X-ray atom labelling scheme.

In this paper, we describe the X-ray structural investigation of the metallation of **1** (or **2**), leading to the zinc(II) complex chloro(2-aza-2-ethoxycarbonylmethyl-5,10,15,20-tetraphenyl-21-carbaporphyrinato-*N*,*N*′*N*″) zinc(II) [Zn(2-NCH$_2$COOC$_2$H$_5$NCTPP)Cl; **4**], the palladium(II) complex (2-aza-2-ethoxycarbonylmethyl-5,10,15,20-tetraphenyl-21-carbaporphyrinato-*N*,*N*′*N*″) palladium(II) [Pd(2-NCH$_2$COOC$_2$H$_5$NCTPP); **5**] and the manganese(III) complex bromo(2-aza-2-ethoxycarbonylmethyl-5,10,15,20-tetraphenyl-21-carbaporphyrinato-*N*,*N*′*N*″) manganese(III) [Mn(2-NCH$_2$COOC$_2$H$_5$NCTPP)Br; **6**] [or the nickel complex 2-aza-(3′-phenoxypropyl)-5,10,15,20-tetraphenyl-21-carbaporphyrinato-*N*,*N*′*N*″) nickel(II)] [Ni(2-NCH$_2$CH$_2$CH$_2$-OC$_6$H$_5$NCTPP); **7**] (Scheme 1).

Klein and co-workers[5] reported the detection of EPR data in S = 2 states of trivalent manganese complexes at an effective g value of 8.7–10. The X-band perpendicular-mode EPR spectra of manganese(III) porphyrins were detected at $g \approx 8$–9 in frozen solutions at 77 K by Talsi and Bryliakov.[6] Hence, the spectrum of the Mn(III) porphyrinoids for **6** is observable in the X-band (only ~9.4 GHz). The new diamagnetic compound **4** is used as a diamagnetic correction for the paramagnetic complex **6** in the solid-state magnetic susceptibility measurements.[7] In this paper, we also focus on the details of the electronic structure of the manganese(III) centre of **6**. Studies on the temperature dependence of the magnetic susceptibility and on the effective moment show that S = 2 is the ground state for the high-spin mononuclear Mn^{3+} centre in **6** at 20 °C. Application of the Van Vleck's equation permits evaluation of D and an average g value for powder samples of **6**.[8]

The peripheral α-carbon [C(3)] is easily oxidized, and the C=N bond [C(3), N(2)] in nickel(II) N-confused porphyrins serves as a dienophile for the Diels–Alder reaction.[9] Notably, the high selectivity of the peripheral carbon–nitrogen bond over the carbon–carbon bonds in metal N-confused porphyrin complexes can be rationalized by the resonance contributions to the overall structures of **5**–**7**. Chart 1 shows two resonance contributors for the two different coordination modes [the formal charge shown for N and C(21) only].[9]

The dipolar canonical form **II** of the C=N in Chart 1(a) is both 'cross conjugated' and in an iminium form which is known to be electron deficient.[10–12] NMR spectroscopy has emerged as a powerful technique for the investigation of the dipolar resonance contributors for species in Chart 1(a).[13] Two groups have shown the NMR spectroscopic studies of iminium ions derived from secondary amines.[14,15] The differentiation of the chemical shifts has been already noticed for two major tautomers of N-confused porphyrin.[11,12] Moreover, the discrimination of the chemical shifts data for the resonance of the dipolar and covalent canonical forms are lacking for metal complexes of N-confused porphyrin. Hence, we reported the ^{1}H and ^{13}C NMR spectroscopic evidence for the dipolar canonical form of iminium ions in metal complexes of N-confused porphyrin **5**–**7** [Chart 1(a)]. The spectroscopic observations are compared with the results of X-ray diffraction analysis. In addition, we compared this work with the results of our recent report on the crystal structures of Pd(2-NCH$_2$C$_6$H$_5$NCTPP) (**10**) and Ni(2-NCH$_2$C$_6$H$_5$NCTPP) (**11**)[16] and with the structures of Ni[2-N(CH$_2$)$_8$I NCTPP] (**12**)[9] and Ni(2-NCH$_2$CH$_2$BrNCTPP) (**13**).[17] For the first time, we combine the data from the δ^{13}C chemical shifts of C(3) and δ^1H

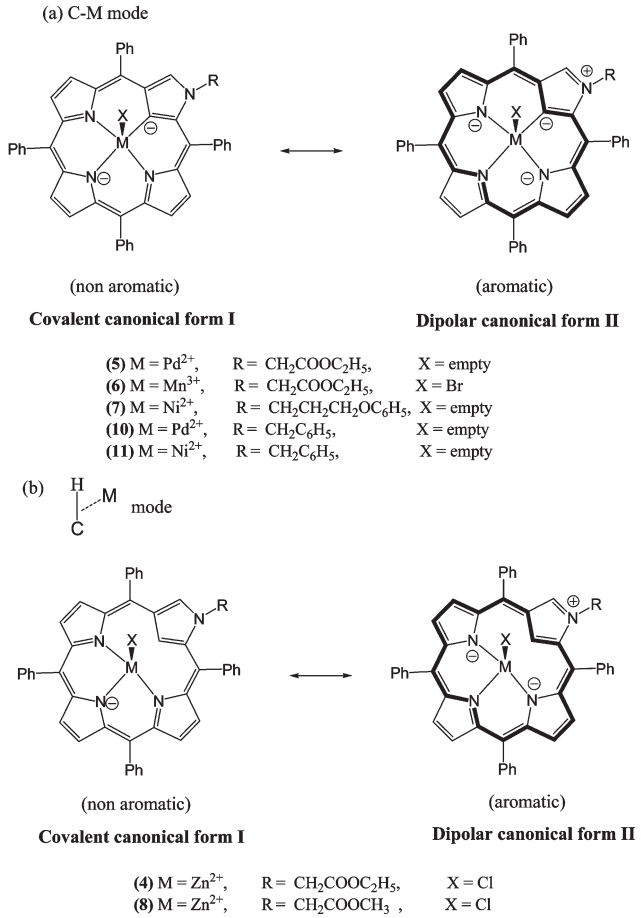

Chart 1 Two resonance contributors for (a) C–M coordination mode and (b) coordination mode of the metal N-confused porphyrin.

chemical shifts of H(3) in Scheme 1 with the X-ray diffraction data of the N(2)–C(3) bond length in metal N-confused complexes giving clear information about which one is the major canonical form responsible for the resonance between the dipolar canonical form **II** and the covalent canonical form **I** in these complexes. The data will show the importance of the canonical form **II** to the so-called resonance hybrid structure in Chart 1(a).

Experimental

Preparation of 2-$NCH_2CH_2CH_2OC_6H_5$NCTPPH (2)

The preparation of **2** is shown in the literature (Fig. S1a in ESI†).[4]

Zn(2-$NCH_2COOC_2H_5$NCTPP)Cl (4) [or 4 (Zn–Et)]

A mixture of **1** (0.03 g, 0.043 mmol) and $ZnCl_2$ (0.03 g, 0.220 mmol) was refluxed in CH_3CN (16 ml) for 12 h.[3] After concentrating the reaction mixture, the residue was dissolved in CH_2Cl_2 (16 ml) and filtered. The filtrate was concentrated and the residue was purified over a silica gel column (230–400 mesh, 50 g) using CH_2Cl_2–EtOAc [10 : 1 (v/v)] as the eluent to yield a green solution of **4**. Removal of the solvent gave **4** as a green solid (0.021 g, 0.026 mmol, 61.2%). Compound **4** was dissolved in CH_2Cl_2 and layered with EtOAc to afford blue crystals for single-crystal X-ray analysis. ^{1}H NMR (599.95 MHz, $CDCl_3$, 20 °C): δ 8.30 [d, H_β(13), ^3J(H–H) = 4.5 Hz]; 8.18 [d, H_β(2), ^3J(H–H) = 5.1 Hz]; 8.13 [d, *o*-H(34, 38), ^3J(H–H) = 6.6 Hz]; 8.06 [d, *o*-H(40, 44), ^3J(H–H) = 7.8 Hz]; 7.76 [d, H_β(3), ^3J(H–H) = 5.1 Hz]; 7.75 [d, H_β(12), ^3J(H–H) = 4.5 Hz]; 7.68 [d, H_β(8), ^3J(H–H) = 5.7 Hz]; 7.62 [d, H_β(7), ^3J(H–H) = 5.7 Hz]; 7.56–7.57 [m, *m*-H & *p*-H]; 6.34 [s, H_α(19)]; 4.51 [d, H(45A) of EtOAc group, ^2J(H–H) = 18.0 Hz]; 4.03 [m, H(47) of EtOAc, ^3J(H–H) = 7.2 Hz]; 4.00 [d, H(45B) of EtOAc group, ^2J(H–H) = 18.0 Hz]; 1.17 [t, H(48) of EtOAc group, ^3J(H–H) = 7.2 Hz]; −0.31 [s, H(17)]. MS(ESI), *m*/*z* (assignment, rel. intensity): 800.66 ($[M]^+$, 67.44%). Anal. Calcd for $C_{48}H_{35}ClN_4ZnO_2$: C, 72.00; H, 4.41; N, 7.00. Found: C, 72.39; H, 4.48; N, 6.96. UV-Vis spectrum, λ (nm) [$\varepsilon \times 10^{-3}$ (M^{-1} cm^{-1})] in CH_2Cl_2: 444 (53.3), 468 (107.2), 579 (9.1), 627 (12.7), 718 (8.7), 785 (28.2) (Fig. S7 in ESI†).

Pd(2-$NCH_2COOC_2H_5$NCTPP) (5) [or 5 (Pd–Et)]

A mixture of **1** (0.03 g, 0.043 mmol) and $PdCl_2$ (0.03 g, 0.141 mmol) was refluxed in CH_3CN (16 ml) for 12 h.[3] After concentrating the reaction mixture, the residue was dissolved in CH_2Cl_2 (16 ml) and filtered. The filtrate was concentrated and the residue was purified over a silica gel column (230–400 mesh, 50 g) using CH_2Cl_2 as the eluent to yield a dark red solution of **5**. Removal of the solvent gave **5** as a dark red solid (0.014 g, 0.017 mmol, 40.3%). Compound **5** was dissolved in CH_2Cl_2 and layered with EtOAc to afford blue-black crystals for single-crystal X-ray analysis. ^{1}H NMR (599.95 MHz, $CDCl_3$, 20 °C): δ 8.15 [s, H_α(19)]; 7.97 [d, H_β(2), ^3J(H–H) = 4.8 Hz]; 7.88 [d, *o*-H(40, 44), ^3J(H–H) = 7.8 Hz]; 7.85 [d, H_β(13), ^3J(H–H) = 6.6 Hz]; 7.81 [d, H_β(8), ^3J(H–H) = 4.8 Hz]; 7.80 [d, H_β(3), ^3J(H–H) = 4.8 Hz]; 7.77 [d, H_β(7), ^3J(H–H) = 4.8 Hz]; 7.74 [d, *o*-H(34), ^3J(H–H) = 6.6 Hz]; 7.72 [d, H_β(12), ^3J(H–H) = 6.6 Hz]; 7.61 [t, *p*-H(36), ^3J(H–H) = 7.8 Hz]; 7.54–7.58 [m, *m*-H & *p*-H]; 7.53 [t, m-H(35,37), ^3J(H–H) = 7.8 Hz]; 4.56 [s, H(45) of EtOAc group]; 4.05 [quintet, H(47) of EtOAc group, ^3J(H–H) = 7.2 Hz]; 1.16 [t, H(48) of EtOAc group, ^3J(H–H) = 7.2 Hz]. MS (ESI), *m*/*z* (assignment, rel. intensity): 804.3 ($[M]^+$, 100%). Anal. Calcd for $C_{48}H_{34}N_4O_2Pd$: C, 71.60; H, 4.26; N, 6.96. Found: C, 71.98; H, 4.18; N 7.16. UV-Vis spectrum, λ (nm) [$\varepsilon \times 10^{-3}$ (M^{-1} cm^{-1})] in CH_2Cl_2: 449 (121.5), 534 (11.5), 576 (9.0), 700 (10.7), 766 (12.6) (Fig. S8 in ESI†).

Mn(2-$NCH_2COOC_2H_5$NCTPP)Br (6) [or 6(Mn–Et)]

A mixture of **1** (0.03 g, 0.043 mmol) and $MnBr_2$ (0.03 g, 0.141 mmol) was refluxed in CH_3CN (16 ml) for 12 h.[3] After concentrating the reaction mixture, the residue was dissolved in CH_2Cl_2 (16 ml) and filtered. The filtrate was concentrated and the residue was purified over a silica gel column (230–400 mesh, 50 g) using CH_2Cl_2–EtOAc [10 : 1 (v/v)] as the eluent to yield a

dark red solution of **6**. Removal of the solvent gave **6** as a dark red solid (0.018 g, 0.022 mmol, 50.3%). Compound **6** was dissolved in CH_2Cl_2 and layered with EtOAc to afford black crystals for single-crystal X-ray analysis. MS(ESI), *m*/*z* (assignment, rel. intensity): 835.2 ([M – ^{81}Br + H]$^+$, 30.38%); 833.2 ([M – ^{79}Br + H]$^+$, 30.53%). Anal. Calcd for $C_{48}H_{34}N_4O_2$-$MnBr{\cdot}CH_3COOCH_2CH_3$: C, 67.76; H, 4.59; N, 6.08. Found: C, 67.96; H, 4.51; N, 6.30. UV-Vis spectrum, λ (nm) [$\varepsilon \times 10^{-3}$ (M^{-1} cm^{-1})] in CH_2Cl_2: 457 (21.2), 474 (18.4), 508 (96.2), 582 (0.2), 753 (1.6) (Fig. S8 in ESI†).

Ni(2-NCH$_2$CH$_2$CH$_2$OC$_6$H$_5$NCTPP) (7)

A mixture of **2** (0.039 g, 0.04 mmol) and $Ni(OAc)_2$ (0.05 g, 0.20 mmol) were refluxed in CH_3CN (10 ml) and CH_2Cl_2 (10 ml) for 12 h.[3,4] After concentrating the reaction mixture, the residue was dissolved in 10 ml of CH_2Cl_2 and filtered. The filtrate was concentrated and the residue was purified over a silica gel column (230–400 mesh, 50 g) using CH_2Cl_2 as the eluent to yield a dark green solution of **7**. Removal of the solvent gave **7** as a purple solid (0.021 g, 0.026 mmol, 65%). Compound **7** was dissolved in CH_2Cl_2 and layered with EtOAc to afford purple crystals for single-crystal X-ray analysis. ^{1}H NMR (599.95 MHz, $CDCl_3$, 20 °C): δ 8.37 [s, H_α(19)]; 7.99 [d, H_β(2), ^3J(H–H) = 4.8 Hz]; 7.93 [d, H_β(7), ^3J(H–H) = 5.1 Hz]; 7.89 [d, H_β(8), ^3J(H–H) = 5.1 Hz]; 7.84 [d, *o*-H (34, 38), ^3J(H–H) = 8.4 Hz]; 7.83 [d, *o*-H (22, 26), ^3J(H–H) = 4.8 Hz]; 7.80 [d, *o*-H (28), ^3J(H–H) = 7.0 Hz]; 7.77 [d, H_β(3), ^3J(H–H) = 4.8 Hz]; 7.76 [d, *m*-H (23), ^3J(H–H) = 4.8 Hz]; 7.62 [d, *o*-H (40, 44), ^3J(H–H) = 7.8 Hz]; 7.60 [d, *o*-H (32), ^3J(H–H) = 7.0 Hz]; 7.56 [m, *p*-H (24)]; 7.56–7.55 [m, *m*-H & *p*-H]; 7.54 [d, *m*-H (35, 37), ^3J(H–H) = 7.8 Hz]; 7.47 [t, *p*-H (42), ^3J(H–H) = 7.8 Hz]; 7.35 [t, *m*-H (41, 43), ^3J(H–H) = 7.2 Hz]; 7.22 [d, *m*-H (50, 52) of phenoxypropyl group, ^3J(H–H) = 8.4 Hz]; 6.96 [t, *p*-H (51) of phenoxypropyl group, ^3J(H–H) = 7.2 Hz]; 6.66 [d, *o*-H (49, 53) of phenoxypropyl group, ^3J(H–H) = 7.8 Hz]; 4.04 [t, H (45) of phenoxypropyl group, ^3J(H–H) = 7.2 Hz]; 3.53 [t, H (47) of phenoxypropyl group, ^3J(H–H) = 5.4 Hz]; 2.00 [quintet, H (46) of phenoxypropyl group, ^3J(H–H) = 7.2 Hz]. MS (ESI), *m*/*z* (assignment, rel. intensity): 805.4 ([M]$^+$, 100%). Anal. Calcd for $C_{53}H_{38}N_4O_2NiO$: C, 79.02; H, 4.75; N, 6.95. Found: C, 79.33; H, 4.67; N 7.00. UV-Vis spectrum, λ (nm) [$\varepsilon \times 10^{-3}$ (M^{-1} cm^{-1})] in CH_2Cl_2: 362 (37.1), 428 (75.1), 462 (40.4), 561 (8.5), 714 (3.9) (Fig. S6 in ESI†).

Zn(2-NCH$_2$COOCH$_3$NCTPP)Cl (8) [or 8 (Zn–Me)]

Compound **4** was dissolved in CH_2Cl_2 and layered with MeOH to afford blue crystals of compound **8** for single-crystal X-ray analysis (Scheme 2).

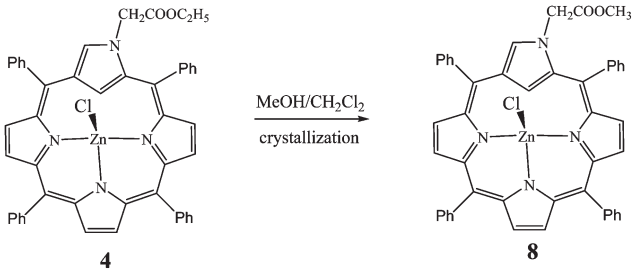

4 **8**

Scheme 2 Alcoholysis of **4**.

^{1}H NMR (599.95 MHz, $CDCl_3$, 20 °C): δ 8.30 [d, H_β(2), ^3J(H–H) = 4.5 Hz]; 8.19 [d, H_β(13), ^3J(H–H) = 4.8 Hz]; 8.14 [d, *o*-H(40, 44), ^3J(H–H) = 7.8 Hz]; 8.06 [d, *o*-H(34, 38), ^3J(H–H) = 7.8 Hz]; 7.78 [d, H_β(12), ^3J(H–H) = 4.8 Hz]; 7.76 [d, H_β(3), ^3J(H–H) = 4.5 Hz]; 7.69 [d, H_β(7), ^3J(H–H) = 5.7 Hz]; 7.62 [d, H_β(8), ^3J(H–H) = 5.7 Hz]; 7.56–7.57 [m, *m*-H & *p*-H]; 6.35 [s, H_α(19)]; 4.53 [d, H(45A) of MeOAc group, ^2J(H–H) = 18.0 Hz]; 4.04 [d, H(45B) of MeOAc group, ^2J(H–H) = 18.0 Hz]; 3.56 [s, H(47) of MeOAc group]; −0.30 [s, H(17)]. MS (ESI), *m*/*z* (assignment, rel. intensity): 786.634 ([M]$^+$, 41.94%). Anal. Calcd for $C_{48}H_{35}ClN_4ZnO_2{\cdot}CH_3OH$: C, 70.42; H, 4.56; N, 6.84. Found: C, 70.45; H, 4.28; N, 6.85. UV-Vis spectrum, λ (nm) [$\varepsilon \times 10^{-3}$ (M^{-1} cm^{-1})] in CH_2Cl_2: 444 (73.3), 466 (157.8), 674 (3.3), 719 (12), 787 (42.4) (Fig. S7 in ESI†).

Magnetic susceptibility measurements

The solid-state magnetic susceptibility was measured under helium on a Quantum Design MPMS5 SQUID susceptometer from 2 to 300 K at a field of 5 kG. The sample was held in a Kel-F bucket. The bucket had been calibrated independently at the same field and temperature. The raw data for **6** were corrected for the molecular diamagnetism. The diamagnetic contribution of the sample was measured from an analogous diamagnetic metal complex **4**. Details of the diamagnetic corrections that were made can be found in ref. 7.

Spectroscopy

The EPR spectra were measured on an X-band Bruker EMX-10 spectrometer equipped with an Oxford Instruments liquid helium cryostat. Magnetic field values were measured with a digital counter. The X-band resonator was a dual-mode cavity (Bruker ER 4116 DM). Proton and ^{13}C NMR spectra were recorded at 599.95 MHz and 150.87 MHz, respectively, on a Varian Unity Inova-600 spectrometer locked on deuterated solvent and referenced to the solvent peak at 20 °C. ^{1}H NMR and ^{13}C NMR are relative to $CDCl_3$ at 7.24 ppm and the center line of $CDCl_3$ at 77.0 ppm, respectively. HMQC (heteronuclear multiple quantum coherence) was used to correlate protons and carbon through one-bond coupling and HMBC (heteronuclear multiple bond coherence) for two- and three-bond protons–carbon coupling. The nuclear Overhauser effect (NOE) difference and ^{1}H–^{1}H COSY spectra were employed to determine the ^{1}H–^{1}H proximity through space over a distance of up to about 4 Å.

The mass spectra [MS(ESI)] were recorded on a Finnigan TSQ Ultra EMR mass spectrometer with an ESI source. UV-Vis spectra were recorded at 20 °C on a Hitachi U-3210 spectrophotometer.

X-Ray crystallography

Table 1 presents the crystal data as well as other information for **4–8**.

Table 1 Crystal data for **4–8**

Empirical formula	$C_{48}H_{35}ClN_4O_2Zn$ (**4**)	$C_{48}H_{34}N_4O_2Pd$ (**5**)	$C_{48}H_{34}BrN_4O_2Mn$ (**6**)	$C_{53}H_{38}N_4NiO$ (**7**)	$C_{47}H_{33}ClN_4O_2Zn$ (**8**)
Formula weight	800.62	805.19	833.64	805.58	786.59
Space group	$P2_1/n$	$P2_1/c$	$P\bar{1}$	$P\bar{1}$	$P2_1/n$
Cryst. system	Monoclinic	Monoclinic	Triclinic	Triclinic	Monoclinic
a/Å	14.4083(5)	10.4698(3)	10.4840(6)	11.8160(5)	11.9685(2)
b/Å	13.4694(5)	25.3342(8)	13.3709(7)	12.3785(5)	14.8500(3)
c/Å	19.7440(6)	15.4465(5)	14.5682(8)	16.3864(7)	23.3388(4)
α/°	90	90	82.570(4)	86.438(4)	90
β/°	100.262(3)	104.940(3)	78.087(4)	83.692(4)	96.174(2)
γ/°	90	90	88.875(4)	66.275(4)	90
V/Å^3	3770.4(2)	3958.6(2)	1981.4(2)	2180.48(16)	4124.0 (1)
Z	4	4	2	2	4
F (000)	1656	1648	852	840	1624
D_c/g cm^{-3}	1.410	1.351	1.397	1.227	1.267
μ/mm^{-1}	0.770	0.513	1.387	0.487	1.753
S	1.038	1.019	1.063	1.011	1.042
Cryst. size/mm^3	0.40 × 0.38 × 0.10	0.60 × 0.30 × 0.12	0.45 × 0.20 × 0.16	0.60 × 0.40 × 0.30	0.60 × 0.40 × 0.20
θ/°	2.87 to 29.23	2.83 to 29.24	2.68 to 29.29	2.99 to 29.30	3.53 to 71.75
T/K	105(2)	110(2)	100(2)	110(2)	110(2)
No. of reflections measured	8701	9145	9172	10 046	7902
No. of reflections observed	6270	5743	5747	6792	6800
R_1 [a]	0.0395	0.0463	0.0738	0.0473	0.0477
wR_2 [b]	0.0995	0.1192	0.2313	0.1320	0.1318

[a] $R_1 = [\sum||F_0| - |F_C||/\sum|F_0|]$. [b] $wR_2 = [\sum w(F_0^2 - F_C^2)^2/\sum w(F_0^2)^2]^{1/2}$.

Measurements for **4–8** were taken on a Oxford Diffraction Gemini S diffractometer using monochromatized Mo Kα radiation (λ = 0.71073 Å). Semi-empirical absorption corrections were made for all complexes. The structures were solved by direct methods (SHELXTL-97)[18] and refined by the full-matrix least-squares method. All non-hydrogen atoms were refined with anisotropic thermal parameters, whereas all hydrogen atoms were placed in calculated positions and refined with a riding model. The C(47) and C(48) atoms within **5** is disordered with an occupancy factor of 0.71 for C(47) C (48) and 0.29 for C(47)′ C(48)′. These C(47) C(48) and C(47)′ C(48)′ were also refined with anisotropic thermal parameters. Tables 2 and 3 list selected bond distances and angles for the five complexes.

Results and discussion

Structures of 4–8

The complexes **4** and **5** were synthesized in 61.2% and 40.3% yields, respectively, by reacting **1** with excess $ZnCl_2$ or $PdCl_2$ in CH_3CN under aerobic conditions (Scheme 1). Complex **6** was produced in 50.3% yield by heating a solution of **1** in CH_3CN under aerobic conditions with an excess of $MnBr_2$ (Scheme 1). Complex **7** was synthesized in 65% yield by reacting **2** with excess $Ni(OAc)_2$ in CH_3CN and CH_2Cl_2 under aerobic conditions. When **4** was dissolved in CH_2Cl_2 and layered with MeOH, a new species was formed that can be formulated as chloro(2-aza-2-methoxycarbonylmethyl-5,10,15,20-tetraphenyl-21-carbaporphyrinato-*N*,*N*′*N*″) zinc(II) [Zn(2-NCH_2COOCH_3-NCTPP)Cl; **8**] (Scheme 2).

The X-ray frameworks of **4–8** are depicted in Fig. 1.

The coordination sphere around the Pd^{2+} (or Ni) ion in **5** (or **7**) is distorted square planar (DSP), and around the Zn^{2+} ion in **4** and **8** is distorted tetrahedron (DT), whereas for Mn^{3+} in **6**, it is distorted square-based pyramid (DSBP) with a Br atom lying in the axial site. Disregarding the axial coordination

Table 2 Selected bond distances (Å) and angles (°) for compounds **4–7**

4			
Zn–N(1)	2.1125(18)	Zn···C(17)	2.513(2)
Zn–N(2)	1.9949(18)	Zn–N(3)	2.1189(18)
Zn–Cl	2.2533(6)	N(4)–C(19)	1.339(3)
N(1)–Zn–N(2)	90.37(7)	Cl–Zn–N(1)	100.59(5)
N(1)–Zn–N(3)	146.51(7)	Cl–Zn–N(2)	118.96(5)
N(2)–Zn–N(3)	89.74(7)	Cl–Zn–N(3)	108.54(5)
5			
Pd–N(1)	2.030(3)	Pd–C(17)	1.955(3)
Pd–N(2)	2.049(3)	Pd–N(3)	2.007(3)
N(4)–C(19)	1.319(5)		
N(1)–Pd–N(2)	90.1(1)	N(1)–Pd–C(17)	90.11(13)
N(1)–Pd–N(3)	177.7(1)	N(2)–Pd–C(17)	176.60(12)
N(2)–Pd–N(3)	90.9(1)	N(3)–Pd–C(17)	89.00(14)
6			
Mn–N(1)	2.050(4)	Mn–C(17)	2.008(5)
Mn–N(2)	2.036(4)	Mn–Br	2.5072(10)
Mn–N(3)	2.036(4)	N(4)–C(19)	1.311(6)
Br–Mn–N(1)	94.00(12)	C(17)–Mn–N(1)	88.27(18)
Br–Mn–N(2)	97.65(12)	C(17)–Mn–N(2)	161.85(18)
Br–Mn–N(3)	102.39(12)	C(17)–Mn–N(3)	87.55(18)
Br–Mn–C(17)	100.49(14)	N(1)–Mn–N(2)	90.22(16)
N(2)–Mn–N(3)	88.83(16)	N(1)–Mn–N(3)	163.56(17)
7			
Ni–N(1)	1.958(2)	Ni–C(17)	1.905(2)
Ni–N(2)	1.962(2)	Ni–N(3)	1.952(2)
N(4)–C(19)	1.326(3)		
N(1)–Ni–N(2)	90.47(8)	N(1)–Ni–C(17)	89.97(9)
N(1)–Ni–N(3)	176.38(8)	N(2)–Ni–C(17)	175.81(9)
N(2)–Ni–N(3)	90.64(8)	N(3)–Ni–C(17)	89.17(9)

environments, the (N, N, N, C) coordination core in **5**, **6** and **7** is retained, while in **4** and **8** they become (N, N, N).

Table 3 Selected bond distances (Å) and angles (°) for compound **8**

8			
Zn–N(1)	2.123(2)	Zn···C(17)	2.566(3)
Zn–N(2)	2.004(2)	Zn–N(3)	2.115(2)
Zn–Cl	2.2642(7)	N(4)–C(19)	1.323(4)
N(1)–Zn–N(2)	89.83(9)	Cl–Zn–N(1)	109.37(6)
N(1)–Zn–N(3)	143.33(9)	Cl–Zn–N(2)	119.57(7)
N(2)–Zn–N(3)	89.03(9)	Cl–Zn–N(3)	102.93(6)

The geometry of the coordination around Mn(III) in **6** is closely related to a square-base pyramid, giving a trigonal distortion parameter (τ) value of 0.03, with Mn(III) being five coordinate, consisting of a N_3CBr donor set.[19] The Mn–C(17), Mn–N(1), Mn–N(2), Mn–N(3) and Mn–Br bond lengths in **6** are 2.008(5), 2.050(4), 2.036(4), 2.036(4) and 2.507(1) Å, respectively. The crystal packing of complex **6** indicates that there are no intermolecular hydrogen bonds linking the individual monomer of **6** into a dimer in the solid state. Complex **6** is monomeric in the solid state.

In **4** and **8**, the geometry about Zn is distorted tetrahedral and the bond distances are as follows: Zn···C(17) = 2.513(2), Zn–N(1) = 2.113(2), Zn–N(2) = 1.995(2), Zn–N(3) = 2.119(2)

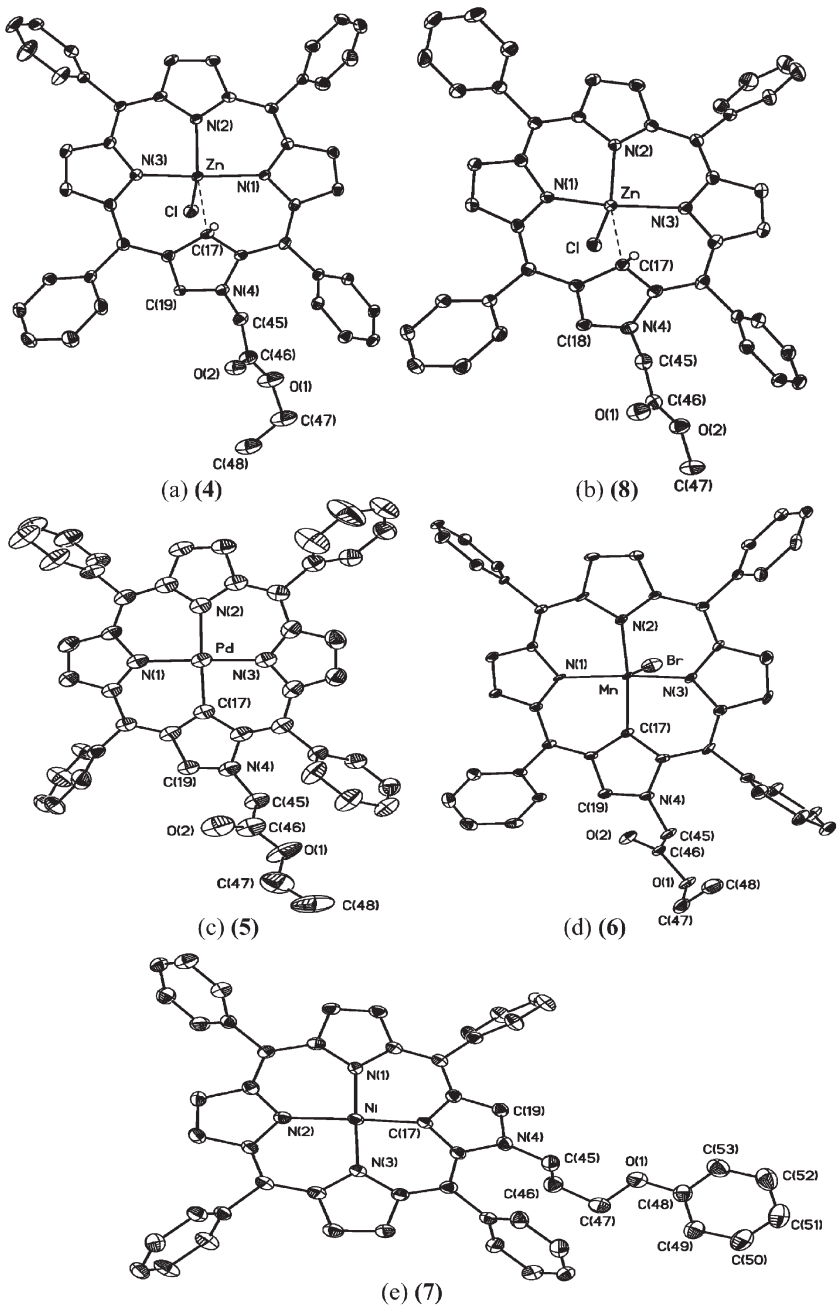

Fig. 1 (a) Molecular structures of **4**, (b) **8**, (c) **5**, (d) **6**, and (e) **7**, with 50% thermal ellipsoids. Hydrogen atoms are omitted for clarity.

and Zn–Cl = 2.2533(6) Å for **4**; Zn···C(17) = 2.566(3), Zn–N(1) = 2.123(2), Zn–N(2) = 2.004(2), Zn–N(3) = 2.115(2) and Zn–Cl = 2.2642(7) Å for **8**. The distance between the inner carbon (17) and the Zn atom 2.513(2) [or 2.566(3) Å] in **4** (or **8**) is short enough for side-on η^1-coordination. A similar distance of 2.53(1) Å was reported by Furuta *et al.* for the Zn(II) NCDPP dimer complex (NCDPP = 5,20-diphenyl-NCP).[20]

In **5** (or **7**), the geometry about Pd (or Ni) is distorted square-planar and the bond distances are as follows: Pd–C(17) = 1.955(3) Å, Pd–N(1) = 2.030(3) Å, Pd–N(2) = 2.049(3) Å and Pd–N(3) = 2.007(3) Å for **5**; Ni–C(17) = 1.905(2) Å, Ni–N(1) = 1.958(2) Å, Ni–N(2) = 1.962(2) Å and Ni–N(3) = 1.952(2) Å for **7**. The average Pd–N and Pd–C distances are 2.029(3) and 1.955(3) Å in **5**, and these are both smaller than those of Pd(II)–N [2.031(2) Å] and Pd(II)–C [1.973(2) Å] in the square-planar Pd(2-NCH$_2$C$_6$H$_5$NCTPP) (**10**) complex.[13] The average Ni–N distance of 1.957(2) in **7** is comparable to the Ni–N distance of 1.955(2) Å in Ni(2-NCH$_2$C$_6$H$_5$NCTPP) (**11**) and the Ni–C distance of 1.905(2) Å in **7** is similar to the Ni–C distance of 1.907(2) Å in complex **11**.[15]

^{1}H NMR spectroscopy data for 4 and 8 in $CDCl_3$

In solution, the ^{1}H NMR spectrum for **4** exhibits seven pyrrole resonances [H_β(13), H_β(12), H_β(2), H_β(3), H_β(8), H_β(7), H_β(17)] (Fig. 1 and 2, and Fig. S2a in ESI†). The doublet at 8.30 ppm is assigned to H_β(13) with ^3J(H–H) = 4.5 Hz and the other doublet at 7.75 ppm is due to H_β(12) with ^3J(H–H) = 4.5 Hz. The doublet at 8.18 ppm is assigned to H_β(2) with ^3J(H–H) = 5.1 Hz and the other doublet at 7.76 ppm is due to H_β(3) with ^3J(H–H) = 5.1 Hz. The doublet at 7.68 ppm is assigned to H_β(8) with ^3J(H–H) = 5.7 Hz and the other doublet at 7.62 ppm is due to H_β(7) with ^3J(H–H) = 5.7 Hz. The signal arising from the H(17) proton of **4** in $CDCl_3$ was observed as a singlet at δ = −0.31 ppm at 20 °C. This observation confirms that there is no coordinated bond between Zn and C(17) in **4**. The geminal protons H(45A) and H(45B) of 2-NCH$_2$COOEtNCTPPH (**1**) in $CDCl_3$ at 20 °C are equivalent and are observed as a singlet at δ = 4.39 ppm. Moreover, these two geminal protons become nonequivalent in complex **4**. Hence the ^{1}H NMR revealed that the geminal protons of H(45A) and H(45B) in **4** appear as a doublet of doublets at 4.51 ppm with ^2J ([H(45A)–H(45B)] = 18 Hz) for H(45A) and has a similar doublet of doublets at 4.00 ppm with ^2J ([H(39A)–H(39B)] = 18 Hz for H(45B).

In solution, the ^{1}H NMR spectrum for **8** exhibits seven pyrrole resonances [H_β(13), H_β(12), H_β(2), H_β(3), H_β(8), H_β(7), H_β(17)] (Fig. 1b, Fig. S2b and S4 in ESI†). The signal arising from the H(17) proton of **8** in $CDCl_3$ was observed as a singlet at δ = −0.30 ppm at 20 °C. The external methyl acetate ligand unit in **8** gave rise to a series of ^{1}H resonances at 4.53 [d, H(45A) of MeOAc group, ^2J(H–H) = 18.0 Hz], 4.04 [d, H(45B) of MeOAc group, ^2J(H–H) = 18.0 Hz] and 3.56 [s, H(47) of MeOAc group].

^{1}H NMR spectroscopy data for 5 and 7 in $CDCl_3$

In solution, the ^{1}H NMR spectrum for **5** exhibits six pyrrole resonances [H_β(12), H_β(13), H_β(7), H_β(8), H_β(2), H_β(3)] (Fig. 1c and 3, and Fig. S3a in ESI†). The doublet at 7.97 ppm is assigned to H_β(2) with ^3J(H–H) = 4.8 Hz and the other doublet at 7.80 ppm is due to H_β(3) with ^3J(H–H) = 4.8 Hz. The doublet

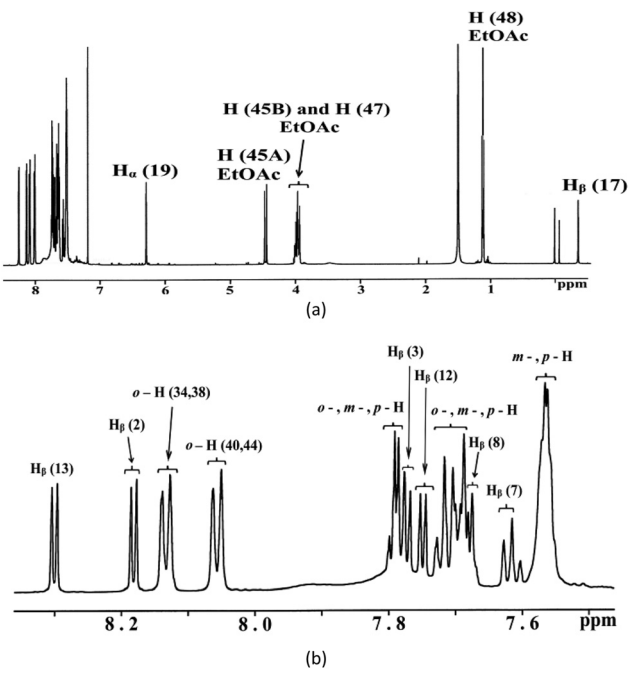

Fig. 2 ^{1}H NMR spectra for **4** at 599.95 MHz in $CDCl_3$ at 20 °C: (a) entire spectrum; (b) expansion of the region 7.50–8.30 ppm in (a) showing seven different β-pyrrole protons H_β and phenyl protons (*o*-H, *m*, *p*-H). Chemical shifts are in ppm from $CDCl_3$ at 7.24 ppm.

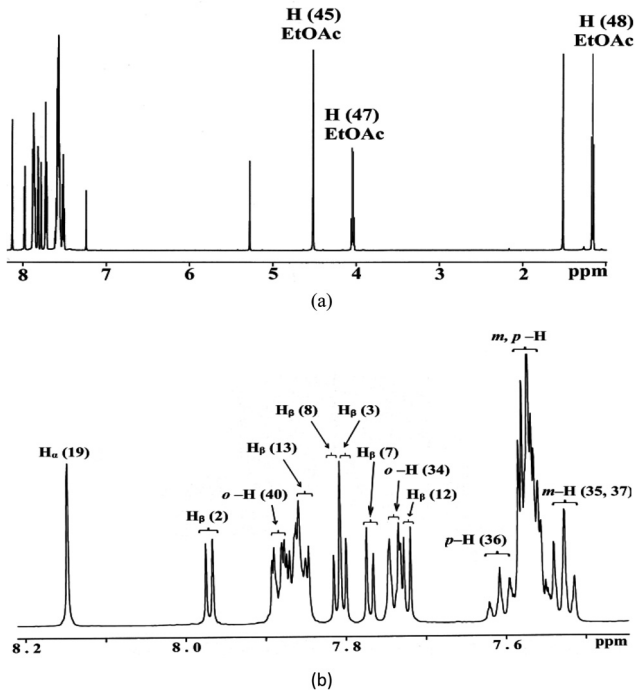

Fig. 3 ^{1}H NMR spectra for **5** at 599.95 MHz in $CDCl_3$ at 20 °C: (a) entire spectrum; (b) expansion of the region 7.50–8.20 ppm in (a) showing six different β-pyrrole protons H_β and phenyl protons (*o*-H, *m*, *p*-H). Chemical shifts are in ppm from $CDCl_3$ at 7.24 ppm.

at 7.85 ppm is assigned to $H_\beta(13)$ with ^3J(H–H) = 6.6 Hz and the other doublet at 7.72 ppm is due to $H_\beta(12)$ with ^3J(H–H) = 6.6 Hz. The doublet at 7.81 ppm is assigned to $H_\beta(8)$ with ^3J(H–H) = 4.8 Hz and the other doublet at 7.77 ppm is due to $H_\beta(7)$ with ^3J(H–H) = 4.8 Hz. The external ethyl acetate ligand unit in **5** gave rise to a series of ^{1}H resonances at 4.56 [s, H(45) of EtOAc group], 4.05 [quintet, H(47) of EtOAc group, ^3J(H–H) = 7.2 Hz], and 1.16 [t, H(48) of EtOAc group, ^3J(H–H) = 7.2 Hz].

In solution, the ^{1}H NMR spectrum for **7** exhibits six pyrrole resonances [$H_\beta(12)$, $H_\beta(13)$, $H_\beta(7)$, $H_\beta(8)$, $H_\beta(2)$, $H_\beta(3)$] (Fig. 1e, Fig. S1b and S5 in ESI†). However, we can only resolve four resonances for H_β. The external phenoxypropyl group unit in **7** gave rise to a series of ^{1}H resonances at 7.22 [d, *m*-H(50, 52), ^3J(H–H) = 8.4 Hz], 6.96 [t, *p*-H(51), ^3J(H–H) = 7.2 Hz], 6.66 [d, *o*-H(49, 53), ^3J(H–H) = 7.8 Hz], 4.04 [t, H(45), ^3J(H–H) = 7.2 Hz], 3.53 [t, H(47), ^3J(H–H) = 5.4 Hz], and 2.00 [quintet, H(46), ^3J(H–H) = 7.2 Hz].

Spin Hamiltonian

The magnetic properties of the high-spin mononuclear Mn(III) ($S = 2$) can be described by the standard spin Hamiltonian ($\hat{H}_S$) comprised of Zeeman and ZFS terms:[5,21–23]

$$(\hat{H}_S) = D\left[S_Z^2 - \frac{1}{3}S(S+1)\right] + E(S_x^2 - S_y^2) + \beta gHS \quad (1)$$

where H is the applied magnetic field, g is the g_{eff}, $S = 2$ is the electronic spin, and D and E are the parameters which describe the effects of the axial and rhombic ligand field, respectively. The zero-field interaction splits the levels of system with $S = 2$ spin into two doublets, one of them is a linear combination of the $m_S = |\pm 2>$ states, *i.e.*, [$|2^+>$, $|2^->$], and the other one of the $m_S = |\pm 1>$ states, *i.e.*, [$|1^+>$, $|1^->$], and a singlet corresponding to the $m_S = |0>$ state, *i.e.*, $|0'>$. As a first approximation, we set E equal to zero.

ESR studies

The X-band (9.374 GHz) ESR spectrum, using parallel polarization, was recorded for a frozen solution of **6** in $CHCl_3$ at 4 K, and is shown in Fig. 4. As has been similarly observed in other Mn(III) complexes, a single line centered at $g_{eff} = 9.54$ is found. This signal is attributed to a formerly forbidden $\Delta M_s = \pm 4$ transition within the $|2^+>$, $|2^->$ non-Kramers doublet for the high-spin mononuclear Mn(III) ($S = 2$) complex of **6** (Fig. 4).[5,6,24,25]

Magnetic properties

Magnetic data for complex **6** are reported in Fig. 5 in the forms of χ_M and μ_{eff} *versus T*.

As can be seen in Fig. 5, the value of μ_{eff} varies from 4.62 μ_B at 300 K to 4.32 μ_B at 2 K. The magnetic moment clearly shows a plateau equal to 4.67 μ_B at high temperature (300–25 K), below which it decreases again. The abrupt rise in μ_{eff} in the range $2 < T < 25$ K is characteristic of compound **6** with significant zero-field splitting (ZFS). The room-temperature effective moment of 4.62 μ_B is lower than the spin-only moment of 4.9 μ_B for an $S = 2$ system, but consistent with that of other high-spin Mn(III) complexes in which $g_{eff} < 2$. Low-symmetry $S = 5/2$ Mn(II) species, which may be present as impurities in Mn(III) compounds, can also give rise to downfield EPR signals near $g = 2$. The data of χ_M *versus T* (or μ_{eff} *versus T*) were inserted into the Van Vleck's equation (eqn (2)) and the term p is the fraction of Mn^{3+}.[8,23]

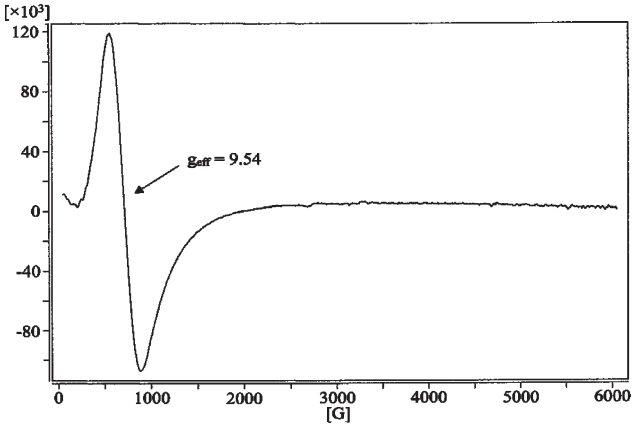

Fig. 4 The X-band ESR spectrum for **6** in $CHCl_3$ at 4 K (parallel polarization). ESR conditions: microwave frequency of 9.374 GHz, microwave power of 15 mW, magnetic field modulation amplitude of 1.60 G, modulation frequency of 100.00 kHz for **6**.

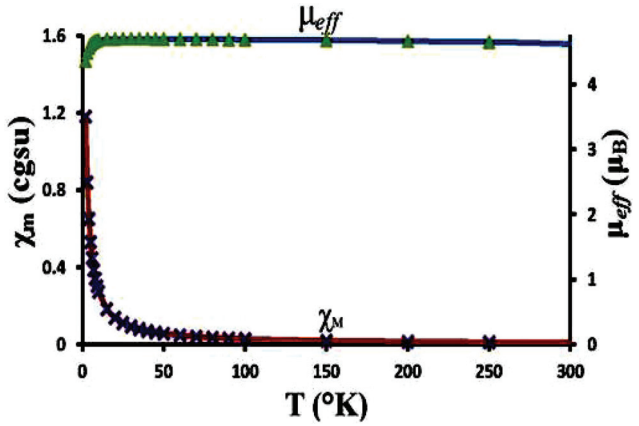

Fig. 5 Temperature variation of the molar magnetic susceptibility (χ_m) and effective magnetic moment (μ_{eff}) for the powder sample of **6**, in the range 2–300 K. Points represent the experimental data; solid lines represent the least-squares fit of the data to eqn (2).

$$\overline{\chi}_M = \frac{0.3749}{T} g^2 \{p \cdot \overbrace{\frac{1}{3}\left[\frac{8 + 2e^{3y} + \frac{1}{y}\left(-\frac{8}{3} - \frac{28}{3}e^{3y} + 12e^{4y}\right)}{2 + 2e^{3y} + e^{4y}}\right]}^{Mn^{3+}} + \underbrace{(1-p)\times 2.917}_{Mn^{2+}(impurity)}\} + TIP \quad (2)$$

where $y = 1.44\frac{D(\mathrm{cm}^{-1})}{T}$ and $\mu_{\mathrm{eff}} = 2.828\sqrt{\chi_{\mathrm{M}}T}$. Here g_{eff} is the effective g value, TIP is the temperature independent paramagnetism and other symbols have their standard meanings. The best fits, as represented in Fig. 5, gave the values of g_{eff} = 1.9, D = −1.63 cm^{-1}, p = 0.947 and TIP = −2.8 × 10^{-4} (cm^3 mol^{-1}), with an agreement factor R of 1.13%.[26] The R value is defined as

$$R = \left\{ \frac{\sum [(\mu_{\mathrm{eff}})_{\mathrm{obsd}} - (\mu_{\mathrm{eff}})_{\mathrm{calcd}}]^2}{\sum (\mu_{\mathrm{eff}})_{\mathrm{obsd}}^{\ 2}} \right\}^{1/2} \times 100\%$$

This $|D|$ value lies near the $1 < |D| < 4.9$ cm^{-1} range found in related Mn(III) porphyrin complexes.

^{1}H and ^{13}C NMR spectroscopy data for the H(3) and C(3) of N=CH(Ar) [or N–CH(Ar)] group in complexes 4–13

Table 4 summarizes the X-ray, ^{1}H and ^{13}C NMR chemical shifts of the N$^+$=CH(Ar) [or N–CH(Ar)] group on the metal complexes **4–13**.

The resonances of the dipolar and covalent forms [Chart 1(a)] have been suggested to explain the observation made in this work.[9,14,27] The comparison of the free ring (**1**) with the dipolar form **II** of Pd complex (**5**) results in a significant deshielding of 17.3 ppm for ^{13}C and 0.96 ppm for ^{1}H of the N$^+$=CH(Ar) group [C(3) and H(3), respectively, Table 4]. The diamagnetic anisotropy from the dipolar form **II** of N$^+$=CH(Ar) in **5** causes the ^{1}H chemical shift of H(3) downfield shift of 0.96 ppm from 7.19 ppm of **1** to 8.15 ppm of **5**.[15,28] A mean electronic excitation energy of ΔE from $\pi \rightarrow \pi^*$ transition of N$^+$=CH(Ar) in **5** in the Karplus–Pople formulation of the ^{13}C screen constant causes the ^{13}C chemical shift of C(3) downfield shift of 17.3 ppm from 135.8 ppm of **1** to 153.1 ppm of **5** (Table 4).[29] The electric field effect originates from molecular dipoles of the dipolar form **II** of $^{\oplus}$N=CH–C=C–C–N$^{\ominus}$ in **5**. For ^{1}H the electric field effect generally produces shifts of less than 0.5 ppm, and for ^{13}C the shifts produced are generally less than 4 ppm.[30] The electric field effect in this work is small and can be disregarded. The similar kind of deshielding were found of 15.2–16.1 ppm (or 16.2 ppm) for ^{13}C and 0.94–1.00 ppm (or 1.1 ppm) for ^{1}H of the N$^+$=CH(Ar) group in complexes **10**, **11** (or complex **7**) (Table 4).[16]

The bond distance between N(2) and C(3) is 1.319(5) Å [or 1.311(6) Å] in **5** (or **6**), shorter than that of compound **1** [1.334(2) Å] by 0.015 Å (or 0.023 Å), respectively (Table 4). Similar phenomena were observed in the X-ray diffraction data of complexes **10**, **11** (or **7**).[16] The bond distances between N(2) and C(3) are 1.311(4), 1.313(3) Å [or 1.326(3) Å] in **10**, **11** (or **7**), shorter than that of compound **9** [1.327(3) Å] [or compound **2** (1.338(2) Å)] by 0.016, 0.014 Å (or 0.012 Å) (Table 4). These bond lengths of 1.311(4)–1.326(3) Å between N(2) and C(3) in Table 3 clearly demonstrate the uniqueness of the N$^+$=CH(Ar) bond with a dipolar canonical form in **5–7**, **10–13** [Chart 1(a)]. The $\Delta\ell = \ell_{\mathrm{N(2)–C(3)\ (metal\ complex)}} - \ell_{\mathrm{N(2)–C(3)\ (free\ ring)}}$ for complexes **4–8**, and **10–11** is shown in Table 4. The metal complexes **5–7**, **10**, **11** with (N, N, N, C) coordination cores indicate that

Table 4 Molecular structures, X-ray, ^{1}H (599.94 MHz) and ^{13}C (150.87 MHz) NMR chemical shifts of the N$^+$=CH(Ar) [or N–CH(Ar)] fragment in $CDCl_3$ for **1**, **4–14**

Compound	δ (^{1}H)[a] (ppm) [C***H***(3)][b]	δ (^{13}C)[a] (ppm) [***C***H(3)][c]	X-Ray dihedral angle φ(°)[d,e] N(22)	N(23)	N(24)	C(21)	X-Ray Coordination geometry[f]	X-Ray N(2)–C(3) (Å)	$\Delta\ell$[g] (Å)	Major canonical form[i]
1[3]	7.19(s)	135.8	11.0	12.8	15.5	25.9[d]	—	1.334 (2)	0	—
4 (Zn–Et)	6.34 (s)	121.2	11.9	3.4	10.3	44.8[d]	DT	1.339(3)	0.005	Covalent
5 (Pd–Et)	8.15 (s)	153.1	5.4	7.0	8.8	8.7	DSP	1.319(5)	−0.015	Dipolar
6(Mn–Et)	—	—	5.1	7.4	4.5	8.3	DSBP	1.311(6)	−0.023	Dipolar
8 (Zn–Me)	6.35 (s)	121.0	13.8	7.0	11.7	45.9[d]	DT	1.323(4)	−0.011	Covalent
2-NCH$_2$CH$_2$CH$_2$OC$_6$H$_5$NCTPPH (**2**)	7.28(s)	136.0	11.4	11.4	16.6	29.9[d]	—	1.338(2)	0	—
Ni(2-NCH$_2$CH$_2$CH$_2$OC$_6$H$_5$NCTPP) (**7**)	8.38(s)	152.2	7.5	7.6	5.5	4.3	DSP	1.326(3)	−0.012	Dipolar
2-NCH$_2$C$_6$H$_5$NCTPPH[16] (**9**)	7.37(s)	136.8	4.4	4.9	12.3	24.3[d]	—	1.327(3)	0	—
Pd(2-NCH$_2$C$_6$H$_5$NCTPP)[16] (**10**)	8.31(s)	152.9	4.8	0.9	3.1	5.5	DSP	1.311(4)	−0.016	Dipolar
Ni(2-NCH$_2$C$_6$H$_5$NCTPP)[16] (**11**)	8.37(s)	152.0	7.8	3.4	2.2	6.6	DSP	1.313(3)	−0.014	Dipolar
Ni[2-N(CH$_2$)$_8$I NCTPP][9] (**12**)	—	—	—	—	—	—	DSP	1.311(4)	—[h]	Dipolar
Ni(2-NCH$_2$CH$_2$BrNCTPP)[17] (**13**)	—	—	9.0	11.3	10.3	10.1	DSP	1.315(6)	—[h]	Dipolar
Pyrrole[31,32] (**14**)	6.74[j]	117.9[j]	—	—	—	—	—	1.365[j]	—	—

[a] The atom labelling for C***H***(3) and ***C***H(3) is shown in Scheme 1. [b] Broad singlet. [c] Singlet. [d] The dihedral angles between the plane defined by N(22) N(23) N(24) and the pyrrole planes [N(22), N(23), N(24), C(21)], respectively, for the free ring in **1**, **2**, **9** and complexes with the (N, N, N) coordination core in **4** and **8**. [e] The dihedral angles between the plane defined by N(22) N(23) N(24) C(21) and the pyrrole planes [N(22), N(23), N(24), C(21)], respectively, for the complexes with the (N, N, N, C) coordination core in **5–7**, **10–13**. [f] DT = distorted tetrahedron, DSP = distorted square planar, DSBP = distorted square-based pyramid. [g] $\Delta\ell = \ell_{\mathrm{N(2)–C(3)\ (metal\ complex)}} - \ell_{\mathrm{N(2)–C(3)\ (free\ ring)}}$, the bond length difference for N(2)–C(3) between the coordination compound and its free ring. [h] Not reported. [i] Two resonances contributors for dipolar form in Chart 1(a) and covalent form in Chart 1(b). [j]

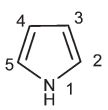

H(2) in pyrrole; C(2) in pyrrole; N(1)–C(2) in pyrrole.

0.012 Å < $|\Delta\ell|$ < 0.023 Å (Table 4). The dihedral angle φ between the C(21) pyrrole plane and the plane defined by N(22) N(23) N(24) C(21) are as follows: 8.7 (**5**), 8.3 (**6**), 4.3 (**7**), 5.5 (**10**), 6.6 (**11**), and 10.1° (**13**). This small dihedral angle φ of 4.3–10.1° in complexes **5–7**, **10**, and **11** indicates that the pyrrole C(21) ring is approximately coplanar with the N(22) N(23) N(24) C(21) plane (Table 4). This coplanarity of the pyrrole C(21) ring enhances both the delocalization of the 18 π-electron aromatic macrocyclic system of NCPs and the formation of the iminium ion for these complexes [Chart 1(a)]. Meanwhile, the peripheral carbon–nitrogen double bonds N^+═CH(Ar) of complexes **5–7**, **10** and **11** are partially isolated from the 18 π-conjugated aromatic system, and ^{13}C and ^1H NMR provides the spectroscopic evidence for the dipolar form **II** of the iminium ions in those complexes.

The change from the free ring (**1**) to the Zn complexes **4** and **8** is associated with a shielding of 14.6–14.8 ppm for ^{13}C and 0.84–0.85 ppm for ^1H of the N–CH(Ar) group [C(3), H(3), respectively, Table 4]. The dihedral angle φ between the C(21) pyrrole plane and the plane defined by N(22) N(23) N(24) in complexes **1**, **2**, **4**, **8** and **9**, are as follows: 25.9° (**1**), 29.9° (**2**), 44.8° (**4**), 45.9° (**8**) and 24.3° (**9**). This large dihedral angle of 44.8–45.9° in complexes **4** and **8** indicates that the pyrrole C(21) ring is highly tilted from the N(22) N(23) N(24) plane (Table 4). This distortion breaks the delocalization of the two lone-pair electrons from N(2) to the N(2)–C(3) bond and inhibits the formation of the iminium ion with a dipolar form in complexes **4** and **8**. Hence the covalent form should be a major canonical form for complexes **4** and **8**, as shown in Scheme 2 and Chart 1(b). Apparently the localization of two double bonds and the large deviation (with φ = 44.8–45.9°) of the pyrrole C(21) plane from their own N(22) N(23) N(24) planes in **4** and **8** makes the pyrrole C(21) planes in these two complexes more like free pyrrole (**14**), shown in Table 4.[31] Complexes **4** and **8** show a ^1H resonance of H(3) in N–CH(Ar) at δ = 6.34 and 6.35 ppm in $CDCl_3$, whereas free pyrrole (**14**) gives a similar signal at δ = 6.74 ppm in the same solvent (Table 4).[32] Complexes **4** and **8** show a ^{13}C resonance of C(3) in N–CH(Ar) at δ = 121.2 and 121.0 ppm in $CDCl_3$, whereas free pyrrole (**14**) also gives a similar signal at δ = 117.9 ppm in $CDCl_3$ (Table 4).[32]

The bond lengths of 1.339(3)–1.324(4) Å between N(2) and C(3) in Table 4 show the existence of the N–CH(Ar) bond with a covalent form in complexes **4** and **8** [Scheme 2 and Chart 1(b)]. Complexes **4** and **8** with (N, N, N) coordination cores show that the absolute value of $\Delta\ell$ is less than 0.011 Å. The dihedral angle of 25.9° (or 29.9°, 24.3°) in complex **1** (or **2**, **9**) indicates that the pyrrole C(21) ring is tilted from its N(22) N(23) N(24) plane. A resonance between the dipolar form and covalent form also exists in the free rings of **1**, **2** and **9**. The covalent form predominates in **1**, **2** and **9**. When the pyrrole C(21) ring in **1** is deviated from its N(22) N(23) N(24) plane and tilted from 25.8° to 44.8° (or 45.9°), and is finally coordinated with the Zn^{2+} ion, it becomes complex **4** (or **8**) with a major covalent form. During this tilt process, the minor amount of the dipolar form of **1** is gradually depleted and causes the ^1H chemical shift of H(3) to undergo an upfield shift of 0.84–0.85 ppm, from 7.19 ppm of **1** to 6.34 ppm (or 6.35 ppm) of **4** (or **8**) (Table 4). In a similar manner, it also causes the ^{13}C chemical shift of C(3) to undergo an upfield shift of 14.6–14.8 ppm, from 135.8 ppm of **1** to 121.2 ppm (or 121.0 ppm) of **4** (or **8**), respectively (Table 4).

According to Table 4, a situation in which the ^{13}C of C(3) and the ^1H of H(3) chemical shifts for the N^+═CH(Ar) fragment are separately located at 152.6 ± 0.5 ppm and 8.30 ± 0.15 ppm suggests that the dipolar form predominates in the diamagnetic metal complexes of 2-N-substituted N-confused porphyrins with (N, N, N, C) coordination cores [Table 4, Chart 1(a)]. In brief, the use of resonance to describe these types of species (**5–7**, **10–13**) has been used to explain why the cross conjugated N-substituted NCPs retain aromatic characteristics. This is emphasized using 2-alkyl NCPs and the closely related azuliporphyrins by Lash and co-workers.[10] The corresponding resonances of the covalent form for the N–CH(Ar) fragment in the diamagnetic metal complexes with (N, N, N) coordination cores were seen at 121.1 ± 0.1 ppm and 6.35 ± 0.01 ppm [Table 4, Chart 1(b)].

X-Ray diffraction data unambiguously indicates that 0.012 Å < $|\Delta\ell|$ < 0.023 Å and N(2)–C(3) 1.315 ± 0.011 Å are found for the dipolar form of **5–7**, **10–13** in Chart 1(a). Meanwhile, the X-ray diffraction data also demonstrates that $|\Delta\ell|$ < 0.011 Å and N(2)–C(3) = 1.331 ± 0.008 Å are observed for the covalent form of **4** and **8** in Chart 1(b).

Conclusions

The peripheral carbon–nitrogen double bonds N^+═CH(Ar) of **5–7**, **10** and **11** are partially isolated from the 18 π-conjugated aromatic system. This work applies, for the first time, the ^{13}C and ^1H chemical shifts to diagnose the dipolar canonical form **II** of the N^+═CH(Ar) group in diamagnetic metal complexes of 2-N substituted N-confused porphyrins. In general, the two ^{13}C and ^1H spectroscopic correlations proposed herein can be applied for diamagnetic metal N-confused complexes.

Acknowledgements

The financial support from the National Science Council of the R. O. C. under grant NSC 101-2113-M-005-013 is gratefully acknowledged. We thank Dr S. Elango for helpful discussions.

Notes and references

1 X. Li, B. Liu, P. Yi, X. Yu and P. J. Chimelewski, *J. Org. Chem.*, 2011, **76**, 2345–2349.
2 T. Ishizuka, H. Yamasaki, A. Osuka and H. Furuta, *Tetrahedron Lett.*, 2007, **63**, 5137–5147.
3 W. Qu, T. Ding, A. Cetin, J. D. Harvey, M. J. Taschner and C. J. Ziegler, *J. Org. Chem.*, 2006, **71**, 811–814.
4 W. C. Lin, D. Z. Hsiao, W. P. Chang, J. H. Chen, S. S. Wang and J. Y. Tung, *Polyhedron*, 2012, **42**, 243–248.
5 S. L. Dexheimer, J. W. Gohdes, M. K. Chan, K. S. Hagen, W. H. Armstrong and M. P. Klein, *J. Am. Chem. Soc.*, 1989, **111**, 8923–8925.
6 E. P. Talsi and K. P. Bryliakov, *Mendeleev Commun.*, 2004, **14**, 111–112.
7 R. S. Drago, *Physical Methods for Chemists*, Saunders College Publishing, New York, 2nd edn, 1992, pp. 473–475, 591–593.
8 R. L. Carlin, *J. Chem. Educ.*, 1966, **43**, 521–525.
9 Z. Xiao, B. O. Patrick and D. Dolphin, *Chem. Commun.*, 2002, 1816–1817.
10 (*a*) T. D. Lash and A. L. V. Ruden, *J. Org. Chem.*, 2008, **73**, 9417–9425; (*b*) T. D. Lash, D. A. Colby, S. R. Graham and S. T. Chaney, *J. Org.*

Chem., 2004, **69**, 8851–8864; (*c*) T. D. Lash, J. A. El-Beck and G. M. Ferrence, *J. Org. Chem.*, 2007, **72**, 8402–8415.
11 P. J. Chmielewski and L. Latos-Grazynski, *J. Chem. Soc., Perkin Trans. 2*, 1995, 503–509.
12 P. J. Chmielewski, L. Latos-Grazynski and T. Glowiak, *J. Am. Chem. Soc.*, 1996, **118**, 5690–5701.
13 M. Fleischmann, D. Drettwan, E. Sugiono, M. Rueping and R. M. Gschwind, *Angew. Chem., Int. Ed.*, 2011, **50**, 6364–6369.
14 H. Mayr, A. R. Ofial, E. U. Wurthwein and N. C. Aust, *J. Am. Chem. Soc.*, 1997, **119**, 12727–12733.
15 C. Rabiller, J. P. Renou and G. J. Martin, *J. Chem. Soc., Perkin Trans. 2*, 1977, 536–541.
16 D. Z. Hsaio, J. H. Chen, S. S. Wang and J. Y. Tung, *Polyhedron*, 2012, **31**, 339–344.
17 I. Schmidt, P. J. Chmielewski and Z. Ciunk, *J. Org. Chem.*, 2002, **67**, 8917–8927.
18 G. M. Sheldrick, *SHELXL-97. Program for Refinement of Crystal Structure from Diffraction Data*, University of Gottingen, Gottingen, Germany, 1997.
19 A. W. Addison, T. N. Rao, J. Reedijk, J. V. Rijn and G. C. Verschoor, *J. Chem. Soc., Dalton Trans.*, 1984, 1349–1356.
20 H. Furuta, T. Morimto and A. Osuka, *Inorg. Chem.*, 2004, **43**, 1618–1624.
21 H. J. Gerritsen and E. S. Sabisky, *Phys. Rev.*, 1963, **132**, 1507–1512.
22 M. P. Hendrich and P. G. Debrunner, *Biophys. J.*, 1989, **56**, 489–506.
23 S. W. Hung, F. A. Yang, J. H. Chen, S. S. Wang and J. Y. Tung, *Inorg. Chem.*, 2008, **47**, 7202–7206.
24 K. P. Bryliakov, D. E. Babushkin and E. P. Talsi, *Mendeleev Commun.*, 1999, **9**, 29–32.
25 J. D. Harvey, C. J. Ziegler, J. Telser, A. Ozarowski and J. Krzystek, *Inorg. Chem.*, 2005, **44**, 4451–4453.
26 A. K. Gregson and N. T. Moxon, *Inorg. Chem.*, 1982, **21**, 581–586.
27 T. D. Lash, D. T. Richter and C. M. Shiner, *J. Org. Chem.*, 1999, **64**, 7973–7982.
28 R. M. Silverstein, F. X. Webster and D. J. Kiemle, *Spectrometric Identification of Organic Compounds*, John Wiley & Sons, New York, 7th edn, 2005, pp. 139–143.
29 F. W. Wehrli, A. P. Marchand and S. Wehrli, *Interpretation of Carbon –13 NMR Spectra*, John Wiley & Sons, New York, 2nd edn, 1989, pp. 34–50.
30 C. H. Yoder and C. D. Schaeffer, *Introduction to Multinuclear NMR*, The Benjamin/Cummings Publishing, California, 1987, pp. 95–96.
31 R. Groddard, O. Heinemann and C. Kruger, *Acta Crystallogr., Sect. C: Cryst. Struct. Commun.*, 1997, **53**, 1846–1850.
32 SDBS No. 481 CDS-00-158, SDBS No. 481 HSP-03-855.